journal

J. Am. Ceram. Soc., **81** [4] 997–1003 (1998)

Role of Microstructure in Hertzian Contact Damage in Silicon Nitride: II, Strength Degradation

Seung Kun Lee*,† and Brian R. Lawn*

Materials Science and Engineering Laboratory, National Institute of Standards and Technology, Gaithersburg, Maryland 20899

In this Part II of a two-part study of the role of microstructure on Hertzian contact damage in silicon nitride we determine strength degradation properties. As previously, three microstructures are investigated: fine (*F*), medium (*M*) and coarse (*C*), representing a progressive transition from brittle to quasi-plastic damage. In both the *F* and *M* materials, failures originate from cone cracks (although limited quasi-plasticity is evident in the latter material). These two materials show abrupt losses in strength at the critical contact loads for cone crack initiation, and steady falloff thereafter at higher contact loads. In the *C* material, failures occur from critical shear faults within the damage ''yield'' zones. The strengths in this material fall off much more gradually, without abrupt drop, above about twice the critical load for the onset of yield. Fracture mechanics models for each type of failure mode provide explicit relations for the degraded strength as a function of contact load. These models account for all the essential features in the observed strength degradation data. Particular attention is given to indenter size effects in the strength responses. Sphere radius has a profound influence on the critical loads for the onset of degradation, but relatively little influence on the degraded strengths at higher loads. Implications of the results concerning contact fatigue and wear are briefly considered.

I. Introduction

In Part I,[1] we characterized the contact responses of silicon nitrides with different degrees of microstructural heterogeneity. There we demonstrated that the mode of damage from Hertzian contacts is fundamentally different in homogeneous and heterogeneous microstructures: in homogeneous, fine-equiaxed grain structures, macroscopic cone cracking (brittle mode); in relatively heterogeneous, coarse-elongate grain structures, distributed microscopic damage (quasi-plastic mode). The quasi-plastic response was shown to be governed by the shear component of the contact field, in the immediate subsurface region where the compressive stresses are triaxial and high. The question now arises: How well do silicon nitride ceramics of each microstructural type retain their strength properties after sustaining contact damage from spherical indenters, especially at high loads? This question, foreshadowed by Makino *et al.*,[2] forms the central theme of this part of the study.

Accordingly, we subject the same silicon nitride materials to strength testing after Hertzian contacts, over a broad range of sphere radii. The study focuses on three controlled silicon nitride microstructures: ''fine'' (*F*), ''medium'' (*M*), and ''coarse'' (*C*).[1] (Recall that, in addition to grain coarsening, the progression $F \rightarrow M \rightarrow C$ also represents increasing $\alpha \rightarrow \beta$ transformation and associated grain elongation.) The two types of contact damage, brittle and quasi-plastic, lead to highly distinct failure modes, from cone cracks in the *F* and *M* materials and from the quasi-plastic zone in the *C* material. Experimental data are represented on strength degradation curves, with inert strength plotted as a function of contact load. The *C* material, although characterized by a lower laboratory strength, shows a much more gradual strength loss with increasing load—it is more ''damage tolerant.'' The results also indicate the important role of sphere size, not so much in the ultimate degraded strength at high loads but in the critical loads at which degradation first becomes manifest.

Basic fracture mechanics models are used to analyze the data for the two damage types, assuming failure directly from a macroscopic cone crack in the *F* and *M* materials and from an individual shear-activated microcrack (''shear fault'') in the *C* material.[3] The models account for the essential data trends in the two material types: in the first type, an abrupt strength loss at the critical load for cone cracking, followed by a slow falloff at higher loading; in the second type, a continuous strength loss above a degradation load well in excess of the load for first yield, followed by an even slower falloff at higher loads. The model allows for an evaluation of the role of sphere size on the strength degradation, and identifies the important material variables for optimum resistance to degradation. It also contains provision for extension to contact fatigue.

II. Experimental Procedure

The silicon nitride materials used here were those described in Part I:[1] (i) ''fine'' (*F*-Si_3N_4), with ≈75 vol% equiaxed α grains of mean size ≈0.4 μm and ≈15 vol% elongated β grains of length 1.5 μm and diameter 0.4 μm; (ii) ''medium'' (*M*-Si_3N_4), with ≈20 vol% equiaxed α grains of mean size ≈0.5 μm and ≈70 vol% elongated β grains of length 4.0 μm and diameter 0.5 μm; (iii) ''coarse'' (*C*-Si_3N_4), elongated β grains of mean length ≈9 μm and diameter 1.5 μm. In each case the structure contained ≈10 vol% interboundary glassy phase.

Hertzian indentations were made in air, using WC spheres of radius $r = 1.59–3.18$ mm, on polished surfaces of prospective tensile specimens, at peak loads up to $P = 4500$ N. Indented surfaces were examined to determine critical loads for onset of fracture and yield, as described in Part I.

Some exploratory Vickers indentations were made at relatively low loads outside the periphery of the Hertzian contact impressions in *C*-Si_3N_4, using the lengths of the radial cracks to assess the magnitude of any long-range residual fields around the macroscopic quasi-plastic zones.

Four-point bend tests were made on bars 3 mm × 4 mm × 25 mm, inner span 10 mm and outer span 20 mm, with the

J. E. Ritter, Jr.—contributing editor

Manuscript No. 191111. Received April 1, 1997; approved July 14, 1997.
Supported by the U.S. Air Force Office of Scientific Research.
*Member, American Ceramic Society.
†Guest Scientist from the Department of Materials Science and Engineering, Lehigh University, Bethlehem, Pennsylvania 18015.

indented surfaces on the tensile side. The edges of the tensile surfaces were prechamfered and polished to minimize edge failures. All specimens were covered by a drop of silicone oil before testing, and were broken in fast fracture (<10 ms), to avoid the influence of moisture (''inert'' strengths). All broken specimens were examined fractographically in Nomarski illumination to locate the source of failure, either indentations or extraneous flaws.

Control strength tests were also made on unindented specimens, to measure baseline ''laboratory'' strengths, as described in Part I.

III. Strength Degradation Curves

In this section we investigate the effects of microstructure and sphere radius on strength degradation, for each of the *F*-Si_3N_4, *M*-Si_3N_4, and *C*-Si_3N_4 materials.

Figure 1 shows broken surfaces of strength test specimens containing indentations made with a WC sphere of radius $r = 2.38$ mm at load $P = 4000$ N. This load is sufficient to produce strength-controlling contact damage in all cases (Part I[1]). Cone cracks are apparent—deep in *F*-Si_3N_4, intermediate in *M*-Si_3N_4, vestigial in *C*-Si_3N_4 (i.e., shallow surface ring cracks). Likewise, quasi-plastic impressions are apparent in *M*-Si_3N_4 and *C*-Si_3N_4, especially in the latter. In the *F* and *M* materials, the final fracture intersects the surface ring crack at a tangent, indicative of failure initiation at the cone base.[4] In the *C* material, on the other hand, the fracture traverses the inner contact zone, passing nearly orthogonal to the vestigial surface ring cracks, indicating a fracture origin from within the subsurface quasi-plasticity zone. The fracture origins are therefore fundamentally different in the two material types. Note that the fracture trace becomes more tortuous through the progression $F \rightarrow M \rightarrow C$, consistent with intergranular fracture in these ever-coarsening structures (Part I).

Results of the indentation–strength tests for the three Si_3N_4 materials are plotted as inert strength σ_F against indentation load P in Figs. 2–4. Data points are individual measured strengths: solid symbols represent specimens that broke at indentation sites; open symbols represent specimens that broke away from indentation sites, i.e., from extraneous flaws. Shaded areas on the left axes are laboratory strengths σ_0 of unindented specimens (Part I). Vertical dashed lines represent threshold loads P_C for cracking (*F*-Si_3N_4 and *M*-Si_3N_4) and P_Y for yield (*M*-Si_3N_4 and *C*-Si_3N_4), and P_D for the onset of degradation for failures from the quasi-plastic zone (*C*-Si_3N_4). Solid curves are fits from the subsequent fracture mechanics analyses (Section IV). The effects of microstructure and contact radius on the strength characteristics are investigated separately below.

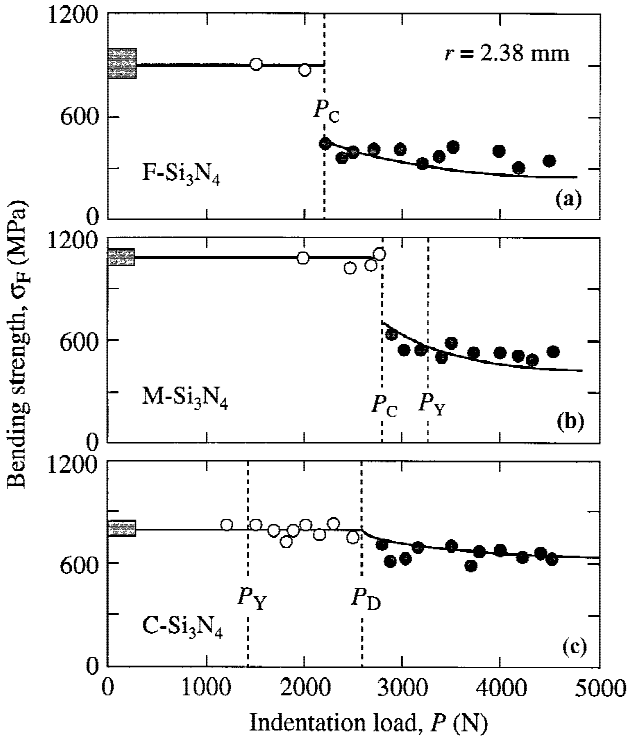

Fig. 2. Inert strength of Hertzian-indented Si_3N_4 specimens indented with WC sphere, $r = 2.38$ mm, as function of indentation load, illustrating effect of microstructure: (a) *F*-Si_3N_4, (b) *M*-Si_3N_4, (c) *C*-Si_3N_4. Data points are experimental measurements, indentation tests in air: closed symbols represent failures from indentation origins, open symbols from other origins. Shaded box at left axis represents strengths of polished, unindented specimens. Vertical dashed lines indicate critical loads P_C, P_Y, and P_D.

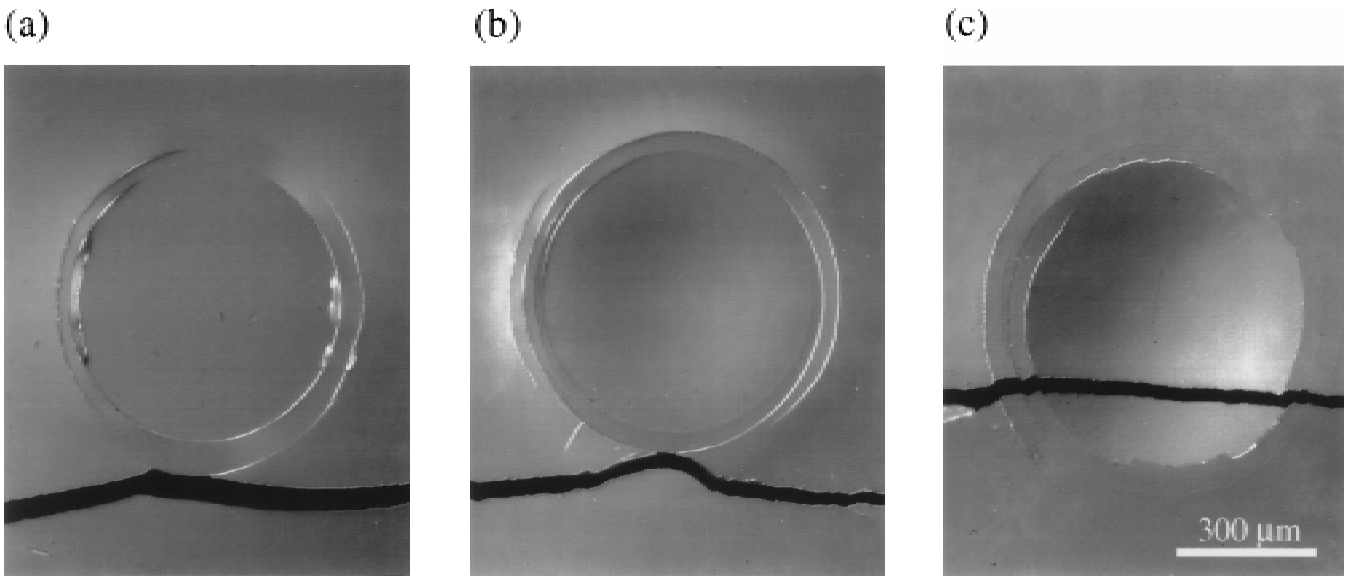

Fig. 1. Micrographs showing failure of silicon nitride specimens in strength tests under inert conditions, for WC sphere radius $r = 2.38$ mm at load $P = 4000$ N, indentation tests in air: (a) *F*-Si_3N_4, (b) *M*-Si_3N_4, (c) *C*-Si_3N_4. Nomarski illumination, surface gold coated. Tensile direction vertical in plane of diagram.

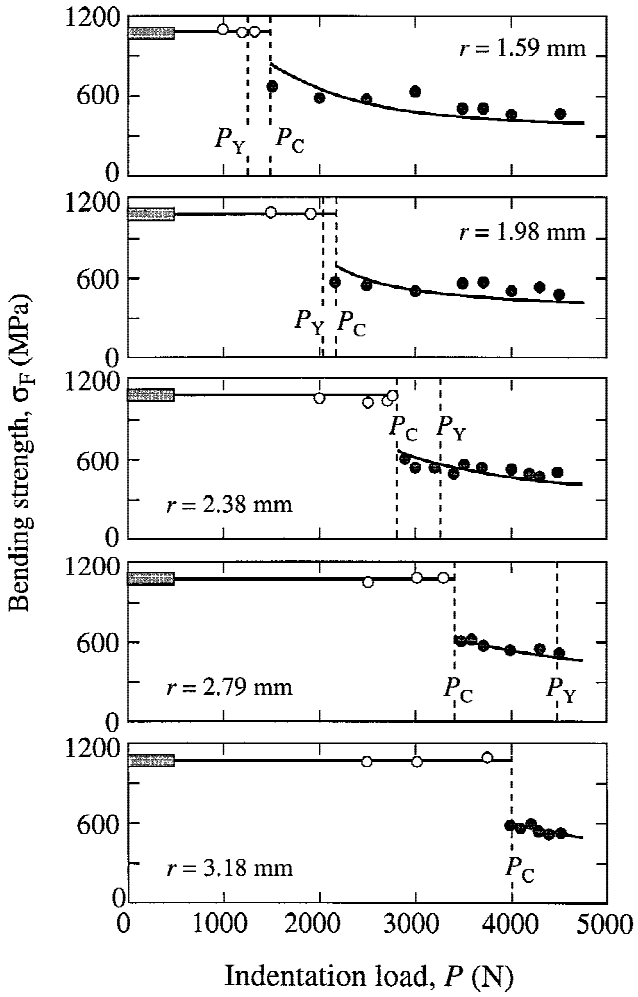

Fig. 3. Inert strength of Hertzian-indented M-Si_3N_4 specimens as function of indentation load, for WC sphere radii r indicated. Data points are experimental measurements, for indentation tests in air: closed symbols represent failures from indentation origins, open symbols from other origins.

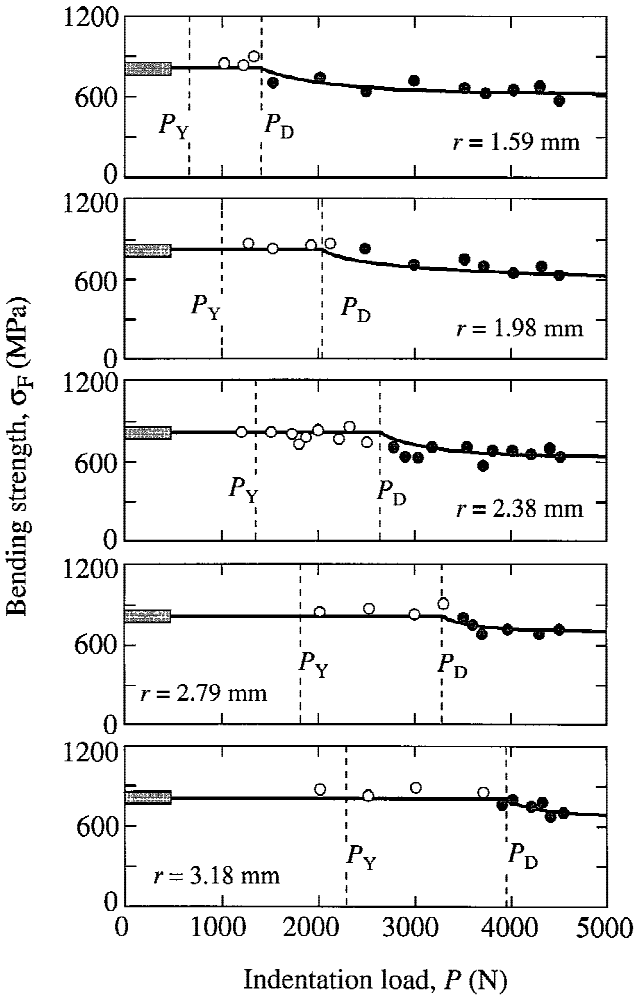

Fig. 4. Inert strength of Hertzian-indented C-Si_3N_4 specimens as function of indentation load, for WC sphere radii r indicated. Data points are experimental measurements, for indentation tests in air: closed symbols represent failures from indentation origins, open symbols from other origins.

The results of exploratory tests using small Vickers indentations in the field of the greater Hertzian contact impressions in C-Si_3N_4 revealed relatively insignificant macroscopic stress intensities from the quasi-plastic zone, ≈125 MPa at the contact periphery, over the sphere radius and contact load ranges studied here (Appendix).

(1) Effect of Microstructure

Figure 2 compares strength degradation data $\sigma_F(P)$ for Hertzian tests on F-Si_3N_4, M-Si_3N_4, and C-Si_3N_4, at a common sphere radius $r = 2.38$ mm. F-Si_3N_4 and M-Si_3N_4 (Figs. 2(a) and 2(b)) show typical brittle responses: no perceptible degradation at $P < P_C$, indicating failures from natural flaws; abrupt dropoff at $P = P_C$, highlighting the effectiveness of cone cracking as a source of strength degradation. The strength continues to fall at $P > P_C$ as the cone cracks are driven deeper with ever-increasing load, but this falloff is relatively slow. In M-Si_3N_4, the incidence of accompanying plasticity at $P > P_Y$ ($>P_C$) has no perceptible effect on the strength (Fig. 1(b)).

C-Si_3N_4 (Fig. 2(c)) shows an altogether different response. The ring cracks are only ''skin deep'' (Fig. 1(c)), and do not cause strength loss. Nor does the onset of plasticity at $P = P_Y$ immediately degrade the strength, even though failures ultimately do occur, at $P = P_D \approx 2P_Y$ in Fig. 1(c), from the quasi-plastic zone. At this point the strength starts to degrade, but without the abrupt falloff seen in F-Si_3N_4 and M-Si_3N_4, and decreases at an even slower rate at higher loads. Thus the quasi-plasticity mode is less deleterious to strength than the traditional cone crack mode. This indicates that the strength properties in C-Si_3N_4 are controlled by less severe flaws, individual shear faults, within the damage zone.[3]

Observe through the sequence $F \rightarrow M \rightarrow C$ in Fig. 2 that the degree of strength loss at the onset of degradation progressively diminishes, and the remaining strength at any given indentation load within the degradation region (closed symbols) progressively increases. Increased quasi-plasticity correlates with enhanced damage tolerance.

(2) Effect of Sphere Radius

Strength degradation data $\sigma_F(P)$ for Hertzian tests in air are plotted in Fig. 3 for M-Si_3N_4 (brittle response) and in Fig. 4 for C-Si_3N_4 (quasi-plastic response), for a range of sphere radii r. The designations on these plots are as in Fig. 2.

For M-Si_3N_4 (Fig. 3), abrupt strength drops are again evident at $P = P_C$. The critical load P_C itself increases monotonically with r. Although the degree of strength dropoff at P_C also increases with r, commensurate with larger popped-in cone cracks, the strengths at $P >> P_C$ tend to similar asymptotic levels. There is no detectable influence from quasi-plasticity, even at $r = 1.59$–2.79 mm where $P_Y < P_C$, confirming that cone cracking remains the dominant mode over the entire radius range studied in this material.

For C-Si_3N_4 (Fig. 4), strength degradation occurs smoothly at $P = P_D$. Note that $P_D \approx 2P_Y$ at all r (P_C for full-scale cone

cracking is off scale). Quasi-plasticity is now the dominant source of failure. Again, whereas P_D is sensitive to r, the degraded strength itself at $P > P_D$ is not. The extremely slow strength falloff in the degradation region again attests to the damage tolerance of this relatively heterogeneous material.

In Fig. 5 we replot the critical loads for first damage and degradation from Figs. 3 and 4 as functions of r. Note that whereas the $P_Y(r)$ curve for M-Si_3N_4 in Fig. 5(a) can be represented by the function $P_Y \propto r^2$, characteristic of a geometrically similar yield process,[5] the $P_C(r)$ curve is somewhat less dependent on r (somewhere between $P_C \propto r^2$ and $P_C \propto r$), indicative of a size dependence in the fracture stress (Part I). Accordingly, the $P_Y(r)$ and $P_C(r)$ curves cross each other (recall Fig. 7, Part I), so the response tends toward an increasing quasi-plasticity component at smaller sphere sizes. On the other hand, the $P_Y(r)$ and $P_D(r)$ curves for C-Si_3N_4 in Fig. 5(b) appear to have the same quadratic dependence, as may be expected for quantities governed by a common quasi-plasticity process, accounting for the near-constant ratio $P_D/P_Y \approx 2$ at all r in Fig. 4.

IV. Mechanics Analysis

As indicated above, the solid curves in Figs. 3 and 4 represent theoretical fits to the strength degradation data. We now briefly summarize the models used to obtain these fits—a detailed analysis is given elsewhere.[3] It is taken that no degradation occurs up to the critical loads P_C or P_D, in accordance with the observations in the previous section. Above these loads failure is assumed to occur from indentation damage, as indicated schematically in Fig. 6: in brittle materials, from fully developed cone cracks (Fig. 6(a)); in quasi-plastic materials, from dominant shear faults within the damage zone (Fig. 6(b)). In each case the aim is to derive analytical expressions for the strength degradation function $\sigma_F(P)$, in terms of underlying material variables.

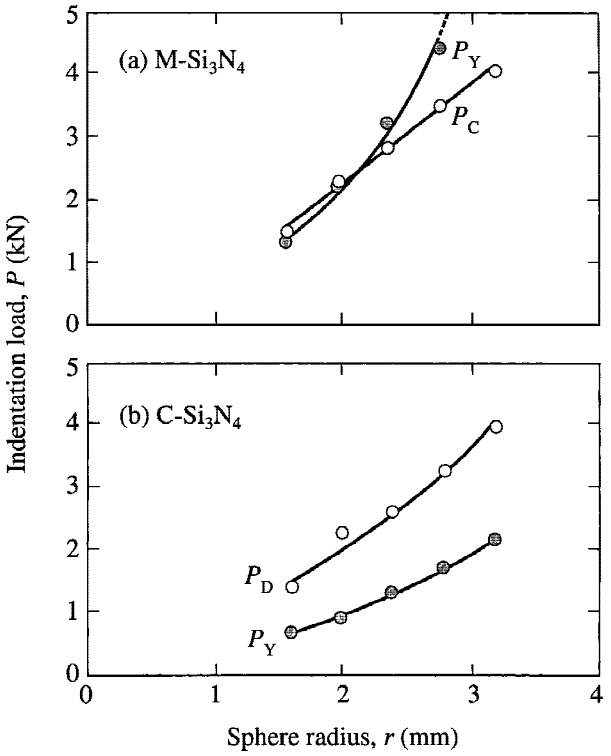

Fig. 5. Critical loads for silicon nitride as function of WC indenter size: (a) M-Si_3N_4, for cone cracking, P_C, and yield, P_Y (from Fig. 7(b), Part I); (b) C-Si_3N_4, for yield, P_Y (Fig. 7(c), Part I), and onset of degradation, P_D.

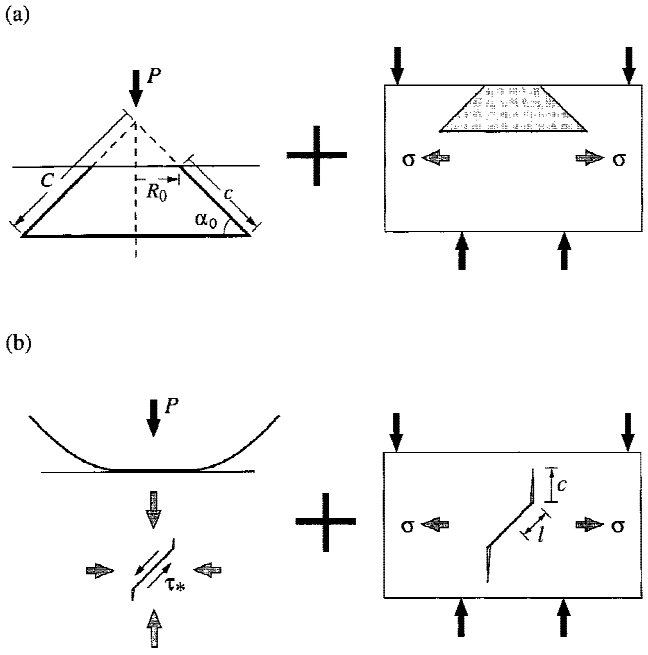

Fig. 6. Schematic showing critical flaws induced by contact with spherical indenter (left), and subsequent strength tests on indented specimens (right): (a) brittle response, failure from fully developed cone crack; (b) quasi-plastic response, failure from shear-fault/wing-crack within damage zone.

(1) Failure from Cone Cracks

For the F-Si_3N_4 and M-Si_3N_4 materials with their brittle responses, we use a simple modification of an analysis developed in an earlier study of Hertzian-induced strength degradation in glass.[6] For materials governed by a single-valued toughness $K_{IC} = T_0$, as is appropriate to both F-Si_3N_4 and M-Si_3N_4 (Part I[1]), and ignoring any macroscopic residual stresses associated with the indentation quasi-plasticity (Appendix), failure occurs spontaneously from a critical crack of size c at tensile stress $\sigma = \sigma_F$ according to the familiar strength relation

$$\sigma_F = T_0/\psi c^{1/2} \tag{1}$$

At $P < P_C$, the strength is governed by the size $c = c_f$ of the preexisting natural flaws (with $\psi = \pi^{1/2}$ for line flaws—cf. Eq. (1) in Part I). In this benign region, σ_F is equal to the laboratory (pre-indentation) strength σ_0, independent of P.

At $P > P_C$, the strength is governed by the size c of the well-developed cone crack, related to the size C of a virtual conical surface with tip located above the indented surface,[6]

$$c = C - R_0/\cos\alpha \tag{2}$$

with α the angle between the cone crack and the specimen surface (Fig. 6(a)). The size C in turn closely satisfies a relation for pennylike cracks (Eq. (3), Fig. 11, Part I),

$$P/C^{3/2} = T_0/\chi \tag{3}$$

with χ a crack geometry coefficient. The requisite strength degradation function $\sigma_F(P)$ may then be solved explicitly from Eqs. (1) to (3). In the asymptotically limiting region of extreme loads at $P >> P_C$ ($c >> R_0/\cos\alpha$), σ_F varies slowly, as $P^{-1/3}$.

While the critical load P_C for cone cracking is relatively dependent on r (somewhere between $P_C \propto r^2$ and $P_C \propto r$, Fig. 5(a)), the degraded strength beyond this point is only slowly dependent. An r dependence in σ_F enters only through Eq. (2), and is important only in the low load region (c comparable with $R_0/\cos\alpha$). Recalling from Part I that $R_0/a_C = 1.15 =$ constant, where a is the contact radius, Hertzian elasticity theory[7,8] gives $R_0 = 1.15(4kP_Cr/3E)^{1/3}$, with E Young's modulus and k an

indenter/specimen elasticity coefficient: so that, if $P_C \propto r^2$, then $R_0 \propto r$; if $P_C \propto r$, then $R_0 \propto r^{2/3}$.

With the data from the cone crack size and geometry characterization in Part I, Eqs. (1) to (3) can be used to predict *a priori* the strength degradation curves for *F*-Si_3N_4 and *M*-Si_3N_4. At $P < P_C$ the values of σ_F are given directly by the laboratory strengths σ_0 (Section II(3), Part I). At $P > P_C$, the cone crack parameters are $\alpha = 19°$ (Section III(3), Part I) and $\chi = 0.0154$ (Section IV(3), Part I). The crack geometry coefficient ψ is determinable from an analysis of crack reinitiation from the cone crack base,[6] yielding $\psi(\alpha) = 0.71$ for $\alpha = 19°$.[3]

The functions $\sigma_F(P)$ from Eqs. (1) to (3) are included as the solid curves for *F*-Si_3N_4 and *M*-Si_3N_4 at $P > P_C$ in Figs. 2 and 3. The predicted strengths pass through the experimental data, within the scatter.

(2) Failure from Quasi-plastic Damage Zones

For the *C*-Si_3N_4 material with its quasi-plastic response, we use a recent model for the strength of solids containing shear-activated microcracks.[3] Specifically, the model assumes that failure occurs from a single pennylike shear fault of radius l with an ''extensile'' wing crack of annular width c at its edges (Fig. 6(b)). The critical shear fault is assumed to be located and oriented so as to experience the maximum principal shear stress within the contact field. Similarly, the wing crack is assumed oriented so as to experience maximum tensile stress within the subsequent flexure field. The system goes to failure when the applied tensile stress is sufficient to drive the equilibrium wing crack to instability.

During contact loading, the fault surfaces slide against frictional tractions, leaving a local residual net shear stress at the fault plane,

$$\tau_* = \tau_P - \tau_c \tag{4}$$

where τ_P is the resolved shear stress on the fault plane at peak load and τ_c is a resistance ''cohesion'' stress. (We omit a possible additional Coulombic contribution to the friction from the resolved compressive stresses across the fault plane.[3,9]) The magnitude of the shear stress $\tau_* = \tau_*(P)$ in Eq. (4) determines the size of the wing cracks.

The driving force from τ_* on the wing cracks persists after contact, and superposes onto the driving force from the subsequent applied tensile stress σ. This driving force is localized at the mouth of the wing crack, and stabilizes the cracks within the superposed tensile field. Accordingly, the wing cracks are predicted to undergo a stage of precursor growth prior to instability, typically by a fault dimension l or so.[3] For materials with single-valued toughness $K_{IC} = T_0$, the equilibrium solution of the composite stress-intensity factor for this stabilized microcrack system yields the strength[3]

$$\sigma_F = (3/4\psi)(T_0^4/4\chi\lambda l^2\tau_*)^{1/3} \tag{5}$$

where ψ (cf. Eq. (1) and λ are crack geometry terms and χ is from Eq. (3). (Strictly, the assumption of single-valued toughness for *C*-Si_3N_4 is not correct, since this material has a rising toughness curve (Fig. 3, Part I); but since the wing crack extensions are relatively small prior to failure, we ignore this complication.)

To obtain the requisite function $\sigma_F(P)$, we need only determine $\tau_*(P)$. This we obtain empirically from FEM analyses of the elastic–plastic contact stress field.[3] Specifically, values of τ_* are evaluated for a fault located at the point of maximum shear stress beneath the contact, at progressively increasing loads P. For indenters which deform elastically, these values can be well represented by the relation[3]

$$\tau_*/\tau_c = \alpha[(P/P_Y)^{1/3} - 1] \qquad (P > P_Y) \tag{6}$$

In Eq. (3), $\sigma_F\tau_*^{1/3} = \sigma_0\tau_D^{1/3} =$ constant defines the net shear stress $\tau_* = \tau_D$ at which the strength σ_F just equals the laboratory strength σ_0, corresponding to $P = P_D$ in Figs. 2 and 4. Insertion of this ''boundary condition'' along with Eq. (6) into Eq. (5) yields

$$\sigma_F = \sigma_0[(P_D^{1/3} - P_Y^{1/3})/(P^{1/3} - P_Y^{1/3})]^{1/3} \qquad (P > P_D) \tag{7}$$

Actually, the WC spheres in our experiments are not ideally elastic, as assumed in Eq. (6), but deform plastically (Part I). However, the sensitivity of Eq. (7) to P is so slow that this is unlikely to lead to serious discrepancy. In any case, plasticity in the indenter will only reduce the value of τ_* in Eq. (6), so that Eq. (7) will, if anything, underestimate the strength (''conservative'' prediction).

The resultant strength–load function $\sigma_F(P)$ for *C*-Si_3N_4, using the curve-fitted functions $P_Y(r)$ and $P_D(r)$ from Fig. 5(b), is included as the solid curves at $P > P_D$ in Figs. 2(c) and 4. (The horizontal lines at $P < P_D$ correspond to the mean laboratory strengths σ_0 for each material.) The fits account for the continuous, ultraslow strength falloff. Note that sphere radius r enters Eq. (7) only through P_D and P_Y (Fig. 5(b)), corresponding to a simple shift along the load axis in Fig. 4.

V. Discussion

In this paper we have presented strength degradation data for three silicon nitride microstructures, nominally fine (*F*), medium (*M*), and coarse (*C*). The response in *F*-Si_3N_4 and *M*-Si_3N_4 is essentially brittle, with failures originating from cone cracks. Conversely, the response in *C*-Si_3N_4 is essentially quasi-plastic, with failures originating from shear faults within the subsurface ''yield'' zone. Analytical models for fitting the data, and for providing a predictive capability for other potential microstructures, have been described. These models are equipped for an account of indentation size effects and for developing design concepts for bearing and other contact configurations.

The foremost interest here is the role of the Si_3N_4 microstructure. *M*-Si_3N_4 represents the compromise structure, with dominant cone cracks but also with partial quasi-plasticity. It is this material that most closely resembles current bearing-grade silicon nitride (Part I[1]). It is stronger than its more brittle counterpart, *F*-Si_3N_4, apparently because it contains a higher fraction of the more resilient β phase, even though it has a coarser grain structure and larger flaw size (Part I). Its drawback is that it still shows a substantial strength drop above the critical load P_C for cone crack initiation (Figs. 2(b) and 3), down to a level of almost one half the laboratory strength. In *C*-Si_3N_4 cone cracking is effectively suppressed, with quasi-plasticity damage dominant. The strength shows no abrupt falloff above the degradation load P_D at which the stable wing cracks associated with the shear faults become the dominant flaws (Figs. 2(c) and 4). The degraded strength is not as low as in *M*-Si_3N_4, even though the starting laboratory strength is considerably lower. Hence the development of pervasive quasi-plasticity below the contact imparts damage tolerance to the silicon nitride microstructure. Potential effects of other variables, such as oxynitride glass composition,[10] are equally amenable to exploration by the contact testing methodology.

The models are explicit in specifying the important material variables in the strength degradation responses for both cone cracking and quasi-plasticity modes. For the brittle materials, high toughness T_0 in Eqs. (1) to (3) is the usual prime requirement for optimum resistance to strength loss from cone cracking. (Low Young's modulus and high Poisson's ratio are secondary requirements, the first to diminish the tensile stresses in the contact field at any given load, and the second to further diminish these stresses and to keep the cone angle α small.[6]) For the quasi-plastic materials, high T_0 is also a factor in Eq. (5) (although the value of T_0 that is pertinent here is the short-crack toughness, which can have an inverse relation with the conventional long-crack toughness[11]). Another factor in the quasi-plastic case is the microstructural fault size l, with inverse dependence in Eq. (5), so that continued coarsening is

expected to enhance the strength degradation. Yet another factor that enters indirectly in Eq. (5), but is of critical importance in the context of fatigue (see below), is the internal friction term τ_c, or yield stress $Y = 2\tau_c$, via τ_* in Eq. (4). Diminishing τ_c increases τ_*, thereby degrading the strength at any given load in Eq. (5). Figure 7 quantifies this degradation in terms of a diminishing ''attrition parameter'' β ($0 \leq \beta \leq 1$), representing the function $\sigma_F(P)$ derived from Eqs. (5) to (7) as before but with τ_c replaced by $\beta\tau_c$ in Eq. (6) (recalling from Eq. (2) in Part I that $P_Y \propto Y^3 \propto \tau_c^3$). From these considerations we may expect that greater microstructural heterogeneity (reducing T_0 and Y, increasing l) is likely to enhance plasticity-induced strength degradation, even while increasing long-crack toughness.[10,12–16]

Another potentially adverse effect of excessively increasing microstructural heterogeneity is enhancement of material removal from the damage zone,[17,18] by coalescence of adjacent wing cracks under extreme loading conditions.[3] Such coalescence is enhanced by the very high local driving stresses from the slipped shear faults (>1 GPa—recall stress–strain curves, Part I) acting on the wing cracks. Considerations of this kind are likely to be important in applications where wear resistance is a major concern. Again, the goals of high toughness and high wear resistance appear to be mutually exclusive. It is on such grounds that the choice of M-Si_3N_4 as a compromise material for bearing applications is physically justifiable.

Figures 3 and 4 demonstrate the strong effect of sphere size in the critical loads for the onset of strength loss, and converse weak effects thereafter in the strength values at higher loads. This distinctive behavior reflects the differences between near fields, which are highly sensitive to local contact conditions, and far fields, which are not.[11,19] For M-Si_3N_4 in Fig. 5(a), there is a trend toward increased quasi-plasticity at smaller sphere sizes, indicative of the size-dependent brittle–ductile transitions that characterize contact fields.[20–22] At very small radii (e.g., $r << 1$ mm),[2] the quasi-plasticity mode will inevitably become the dominant source of degradation in M-Si_3N_4 ($P_Y << P_C$), and, ultimately, even in the ostensibly brittle F-Si_3N_4 (Part I). At this microcontact level where the stress concentrations are high the quasi-plastic zones can be accompanied by the radial cracks that typify ''sharp'' indenters.[2,23]

We have alluded to the relevance of the strength degradation data to the issues of damage tolerance. It is well established that the laboratory strengths of homogeneous materials are much more sensitive to extraneous flaws than those of heterogeneous materials.[24] The critical loads for cone cracking are also more sensitive to extraneous flaws, especially surface finish flaws,[6] than the critical loads for yield, since the latter process occurs subsurface. We have also seen in Figs. 2–4 how F-Si_3N_4 and M-Si_3N_4 are much more susceptible to abrupt strength losses than is C-Si_3N_4. (Similar flaw sensitivities are observed in strength data on fine and coarse silicon nitrides subjected to thermal shock.[15]) Moreover, in C-Si_3N_4 the losses do not occur until well above the first signs of damage, i.e., $P_D \approx 2P_Y$. Unlike their homogeneous counterparts, the heterogeneous materials are capable of sustaining substantial distributed, and detectable, damage before strength is impaired. This raises the prospect of an ''early warning'' prior to component failure, opening the possibility of nondestructive evaluation.

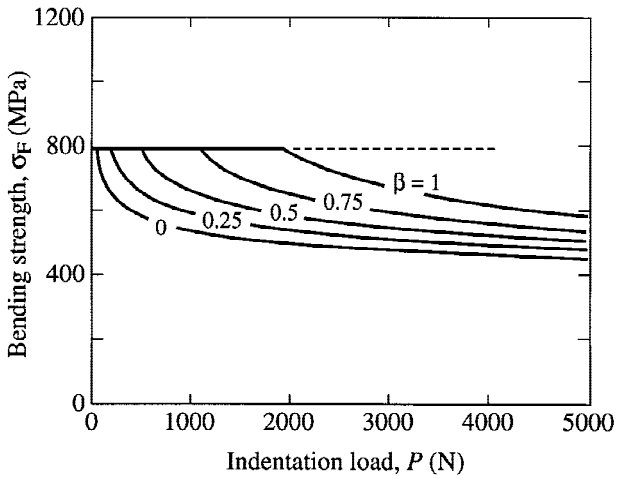

Fig. 7. Hypothetical strength–load functions for C-Si_3N_4, for various values of attrition parameter β, illustrating effect on strength of diminished frictional resistance $\beta\tau_c$ (see text).

Of the two damage models described in Section IV, that for cone cracking in brittle materials is more amenable to *a priori* predictions of strength degradation behavior. That is because the cone-crack dimensions and geometry in Eqs. (1) to (3) are readily ''calibrated'' by direct measurement (Part I). The shear-fault/wing-crack model for quasi-plastic materials requires an empirical determination of P_D in Eq. (7) from the actual strength degradation data, so the data analysis represents more a fit than a prediction. Experimentally, it is not so simple to ''calibrate'' the microscopic wing-crack configurations from direct measurements, thus necessitating the empirical fitting routine. And since the models are subject to several assumptions and approximations, including the assumption that the toughness remains single-valued (even in the C-Si_3N_4—see Part I), evaluations of material variables from these parameters fits should not be taken too literally.[3] This caution extends to the predicted forms of the strength degradation functions—on the other hand, since the $\sigma_F(P)$ data are slowly varying in Figs. 2–4, such uncertainties are unlikely to be an important limitation in the modeling.

Finally, we acknowledge the restriction of the present study to single-cycle contacts, and to comparatively innocuous laboratory atmospheres. The Hertzian testing procedure is readily extendible to multiple-contact loading, under any specifiable adverse chemical environment, and thus to the study of accelerated strength degradation from contact fatigue.[17,18,25–27] Any such fatigue in highly brittle solids would appear to be exclusively *chemical*, from water-assisted slow growth crack of the cone cracks, by reducing P_C and enhancing c in Eqs. (1) to (3).[17] Slow crack growth could also enhance the growth of wing cracks in quasi-plastic materials, if water were to gain access to the subsurface shear faults, as would certainly ensue if any microcrack coalescence were to occur. Deleterious effects of water in contact fatigue tests have been well demonstrated in coarse-grain alumina.[25] But potentially more damaging in the heterogeneous materials is *mechanical* fatigue, from reductions in friction stress τ_c (and μ) at the repeatedly sliding shear fault surfaces.[18] This mode of fatigue has been demonstrated strikingly at multiple-contact sites in heterogeneous silicon carbide, as attritional surface debris within the contact damage zone, and ultimately as excessive material spalling,[17] and has been foreshadowed in earlier contact tests on silicon nitride.[28] A more detailed study of the role of microstructure in contact fatigue of silicon nitride is under way.

APPENDIX

Evaluation of Macroscopic Residual Stresses around Hertzian Impressions Using Exploratory Vickers Indents

In this Appendix we describe evaluations of macroscopic residual stresses around the quasi-plastic Hertzian impressions in C-Si_3N_4, using simple exploratory Vickers tests. This test has been employed by Makino *et al.*[2] to explore around Hertzian impressions made with a harder (diamond) and much smaller ($r \approx 200$ μm) sphere than used here (WC, $r > 1$ mm), in a coarse silicon nitride material analogous to our C-Si_3N_4. The contact impressions in that study represent much higher contact pressures, as indicated by strong anisotropy in the Vickers radial crack patterns, than in our present work (note

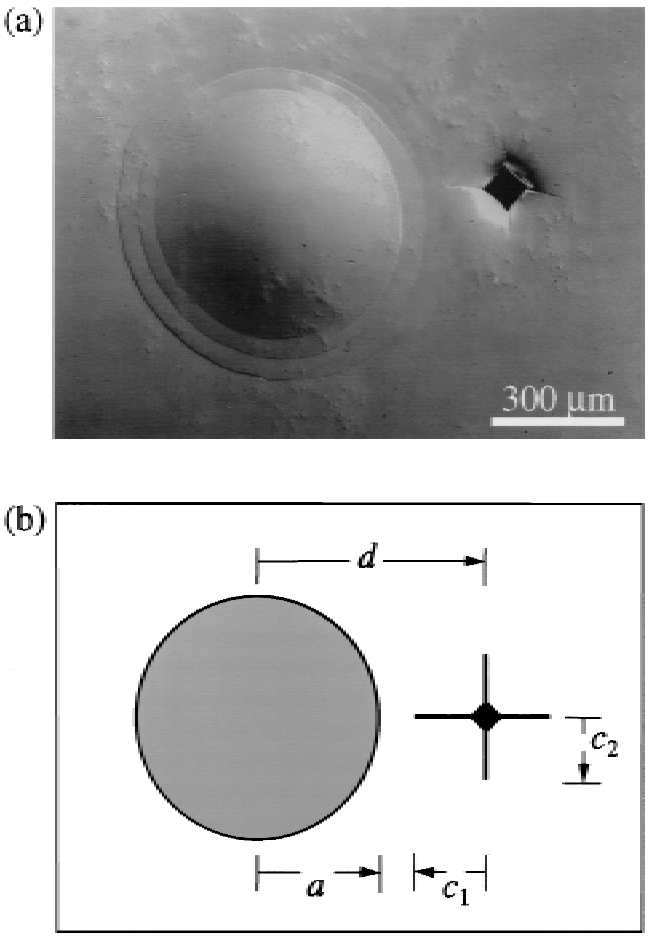

Fig. A1. Exploratory Vickers indentation, formed at load 100 N, in field of preceding Hertzian impression, formed at load 4000 N with WC sphere of radius $r = 1.98$ mm: (a) micrograph, showing slightly larger Vickers radial crack length for arm closest to Hertzian impression; (b) schematic, showing coordinate system used to evaluate macroscopic residual Hertzian stress field.

from Fig. 4, Part I, that the indentation stress–strain curve in our *C*-Si_3N_4 does not approach hardness saturation over the range of contact conditions covered).

Figure A1(a) shows a 100 N Vickers indentation made on the surface of a *C*-Si_3N_4 specimen previously indented with a WC sphere of radius $r = 1.98$ mm at a relatively high load $P = 4000$ N (cf. Fig. 4). Figure A1(b) indicates the coordinate system used to quantify the test. The Vickers indentation in Fig. A1 is located at a radial distance $d = 520$ μm from the center of Hertzian contact, relative to the impression radius $a = 333$ μm. The radial cracks at the corners of the Vickers indent show comparatively small asymmetry, $c_1 = 133$ μm vs $c_2 = 124$ μm.

To a first approximation, the radial and tangential components of the stress field around the residual contact field at radial distance $d > a$ are given by[29]

$$\sigma_r = -\sigma_a(a/d)^3, \qquad \sigma_t = \tfrac{1}{2}\sigma_a(a/d)^3 \tag{A-1}$$

where σ_a is the radial stress at the impression periphery, $d = a$. These macroscopic stresses contribute to the net stress-intensity factors on the Vickers radial cracks, superposing onto the residual stress term from the Vickers elastic–plastic field. Ignoring stress gradients along the radial crack lengths, we have

$$K = \chi_V P/c_1^{3/2} + \tfrac{1}{2}\psi_V\sigma_a(a/d)^3c_1^{1/2} = T_0 \tag{A-2a}$$

$$K = \chi_V P/c_2^{3/2} - \psi_V\sigma_a(a/d)^3c_2^{1/2} = T_0 \tag{A-2b}$$

at equilibrium, where χ is a material-dependent coefficient, the subscript V denoting the Vickers configuration. From measurements on 10 Vickers indentations under the same load conditions as specified in Fig. A1, but at various values of ratio *d/a*, Eqs. (A-2) yield $\sigma_a \approx -125 \pm 20$ MPa, which we consider negligible relative to the much larger values of *local* residual stresses about the shear faults (>1 GPa) referred to in the text.

Acknowledgment: We wish to thank Sataporn Wuttiphan, Irene M. Peterson, Kee Sung Lee, and Nitin P. Padture for helpful discussions.

References

[1]S. K. Lee, S. Wuttiphan, and B. R. Lawn, ''Role of Microstructure in Hertzian Contact Damage in Silicon Nitride: I, Mechanical Characterization,'' *J. Am. Ceram. Soc.*, **80** [9] 2367–81 (1997).
[2]H. Makino, N. Kamiya, and S. Wada, ''Effects of Grain Size of Hot-Pressed Silicon Nitride on Contact Damage Morphology and Residual Strength,'' *J. Am. Ceram. Soc.*, **74** [8] 2001–2004 (1991).
[3]B. R. Lawn, S. K. Lee, I. M. Peterson, and S. Wuttiphan, ''A Model of Strength Degradation from Hertzian Contact Damage in Tough Ceramics,'' *J. Am. Ceram. Soc.*, in press.
[4]B. R. Lawn, S. M. Wiederhorn, and D. E. Roberts, ''Effect of Sliding Friction Forces on the Strength of Brittle Materials,'' *J. Mater. Sci*, **19**, 2561–69 (1984).
[5]D. Tabor, *Hardness of Metals.* Clarendon, Oxford, U.K., 1951.
[6]B. R. Lawn, S. M. Wiederhorn, and H. Johnson, ''Strength Degradation of Brittle Surfaces: Blunt Indenters,'' *J. Am. Ceram. Soc.*, **58** [9–10] 428–32 (1975).
[7]K. L. Johnson, *Contact Mechanics*. Cambridge University Press, London, U.K., 1985.
[8]S. Timoshenko and J. N. Goodier, *Theory of Elasticity.* McGraw-Hill, New York, 1951.
[9]B. R. Lawn and D. B. Marshall, ''Nonlinear Stress–Strain Curves for Solids Containing Closed Cracks With Friction,'' *J. Mech. Phys. Solids*, **46** [1] 85–113 (1998).
[10]P. F. Becher, S. L. Hwang, H. T. Lin, and T. N. Tiegs, ''Microstructural Contributions to the Fracture Resistance of Silicon Nitride Ceramics''; pp. 87–100 in *Tailoring of Mechanical Properties of Si_3N_4.* Edited by M. J. Hoffmann and G. Petzow. Kluwer Academic Publishers, Dordrecht, Netherlands, 1994.
[11]B. R. Lawn, *Fracture of Brittle Solids.* Cambridge University Press, Cambridge, U.K., 1993.
[12]C.-W. Li and J. Yamanis, ''Super-Tough Silicon Nitride with *R*-Curve Behavior,'' *Ceram. Eng. Sci. Proc.*, **10** [7–8] 632–45 (1989).
[13]N. Ramachandran and D. K. Shetty, ''Rising Crack-Growth-Resistance (*R*-Curve) Behavior of Toughened Alumina and Silicon Nitride,'' *J. Am. Ceram. Soc.*, **74** [10] 2634–41 (1991).
[14]C.-W. Li, D.-J. Lee, and S.-C. Lui, ''*R*-Curve Behavior and Strength of *In Situ* Reinforced Silicon Nitride with Different Microstructures,'' *J. Am. Ceram. Soc.*, **75** [7] 1777–85 (1992).
[15]M. J. Hoffmann, ''Analysis of Microstructural Development and Mechanical Properties of Si_3N_4''; pp. 59–72 in *Tailoring of Mechanical Properties of Si_3N_4.* Edited by M. J. Hoffmann and G. Petzow. Kluwer Academic Publishers, Dordrecht, Netherlands, 1994.
[16]C.-W. Li, S.-C. Lui, and J. Goldacker, ''Relation Between Strength, Microstructure, and Grain-Bridging Characteristics in *In Situ* Reinforced Silicon Nitride,'' *J. Am. Ceram. Soc.*, **78** [2] 449–59 (1995).
[17]N. P. Padture and B. R. Lawn, ''Contact Fatigue of a Silicon Carbide with a Heterogeneous Grain Structure,'' *J. Am. Ceram. Soc.*, **78** [6] 1431–38 (1995).
[18]N. P. Padture and B. R. Lawn, ''Fatigue in Ceramics with Interconnecting Weak Interfaces: A Study Using Cyclic Hertzian Contacts,'' *Acta Metall.*, **43** [4] 1609–17 (1995).
[19]B. R. Lawn and T. R. Wilshaw, ''Indentation Fracture: Principles and Applications,'' *J. Mater. Sci.*, **10** [6] 1049–81 (1975).
[20]B. R. Lawn and D. B. Marshall, ''Hardness, Toughness, and Brittleness: An Indentation Analysis,'' *J. Am. Ceram. Soc.*, **62** [7–8] 347–50 (1979).
[21]K. E. Puttick, ''Energy Scaling, Size Effects and Ductile–Brittle Transitions in Fracture,'' *J. Phys. D: Appl. Phys.*, **12**, L19–23 (1979).
[22]K. Puttick, ''The Correlation of Fracture Transitions,'' *J. Phys. D: Appl. Phys.*, **13**, 2249–62 (1980).
[23]B. R. Lawn, E. R. Fuller, and S. M. Wiederhorn, ''Strength Degradation of Brittle Surfaces: Sharp Indenters,'' *J. Am. Ceram. Soc.*, **59** [5–6] 193–97 (1976).
[24]S. J. Bennison, N. P. Padture, J. L. Runyan, and B. R. Lawn, ''Flaw-Insensitive Ceramics,'' *Philos. Mag. Lett.*, **64** [4] 191–95 (1991).
[25]F. Guiberteau, N. P. Padture, H. Cai, and B. R. Lawn, ''Indentation Fatigue: A Simple Cyclic Hertzian Test for Measuring Damage Accumulation in Polycrystalline Ceramics,'' *Philos. Mag.*, **A68** [5] 1003–16 (1993).
[26]H. Cai, M. A. S. Kalceff, B. M. Hooks, B. R. Lawn, and K. Chyung, ''Cyclic Fatigue of a Mica-Containing Glass-Ceramic at Hertzian Contacts,'' *J. Mater. Res.*, **9** [10] 2654–61 (1994).
[27]A. Pajares, L. Wei, B. R. Lawn, and D. B. Marshall, ''Damage Accumulation and Cyclic Fatigue in Mg-PSZ at Hertzian Contacts,'' *J. Mater. Res.*, **10** [10] 2613–25 (1995).
[28]H. H. K. Xu, L. Wei, N. P. Padture, B. R. Lawn, and R. L. Yeckley, ''Effect of Microstructural Coarsening on Hertzian Contact Damage in Silicon Nitride,'' *J. Mater. Sci.*, **30**, 869–78 (1995).
[29]J. Selsing, ''Internal Stresses in Ceramics,'' *J. Am. Ceram. Soc.*, **44** [8] 419 (1961). □